Mössbauer-effect study of iron-boron-beryllium metallic glasses

M. C. Lin, C. S. Severin, R. G. Barnes, and C. W. Chen
Ames Laboratory-U.S. Department of Energy and Departments of Physics and Materials Science and Engineering, Iowa State University, Ames, Iowa 50011
(Received 27 April 1981)

^{57}Fe Mössbauer spectra have been obtained at both liquid-nitrogen and room temperatures for a series of metallic glasses $Fe_{82}B_{18-x}Be_x$ with $0 \leq x \leq 6$. With the use of Window's program the spectra were fitted and deconvoluted to obtain the probability distribution function of the effective magnetic hyperfine field $P(H)$, and the results show a well-defined symmetric shape for these metallic glasses. The width of $P(H)$, ΔH, remains approximately constant at a value of 80 kOe for all samples. However, the most probable value of the effective magnetic hyperfine field H_1 at liquid-nitrogen temperature initially increases with the Be content to 4 at.%, but starts to decrease as x exceeds 4. The isomer shift has a value of -0.032 mm/sec for samples with $x \leq 4$ but changes to -0.050 mm/sec for samples with $x > 4$. The crystallization products obtained upon annealing the $Fe_{82}B_{18}$ metallic glass at $T_a = 420\,^{\circ}C$ were identified as tetragonal Fe_3B and α-Fe. The annealing of the samples with $x > 0$ between T_{x1} and T_{x2} yields a metastable amorphous phase and crystalline solid solutions of an Fe-Be phase. Annealing of the samples with $x > 0$ above T_{x2} yields crystalline Fe-Be solid solutions and the Fe_2B intermetallic compound. The intensity ratios in the Mössbauer spectra clearly indicate that annealing of samples between T_{x1} and T_{x2} led to the alignment of the $\overline{H}_{\text{eff}}$ direction close to the ribbon plane, but annealing above T_{x2} left $\overline{H}_{\text{eff}}$ randomly oriented.

I. INTRODUCTION

Metallic glasses have recently generated both fundamental and practical interests because of their useful mechanical and soft magnetic properties and very high electrical resistivity. Structural analyses by x-ray diffraction of many metallic glasses have indicated that the atomic distribution can be considered as a random packing of hard spheres.[1,2] As a result, physical properties which are sensitive to the local configuration will have a distribution of values. In principle, the Mössbauer effect of ^{57}Fe can be used effectively to study the short-range atomic arrangements because the magnetic hyperfine field present at iron sites is strongly dependent on the local environment. Indeed, such a study has been carried out in detail for Fe-B, Fe-P-B, and Fe-Ni-P-B metallic glasses.[3–5]

Since metallic glasses are in a metastable state, irreversible transformation into the stable cyrstalline state should occur upon heating above the crystallization temperature. The crystallization processes are dependent on both temperature and time. The study of crystallization behavior of metallic glasses will not only provide information on thermal stability of the glasses but also give some insight into the nature of metallic glasses. Mössbauer spectroscopy has been successfully used to study crystallization processes and their products.[3,6] From those studies interesting results about the structure and thermal stability of amorphous materials were obtained.

The majority of the reported metallic glasses are transition metal (TM)-metalloid (M) systems with TM being Fe, Ni, or Co and M being B, P, C, Si, or Ge. A new metallic glass system, $Fe_{82}B_{18-x}Be_x$ ($0 \leq x \leq 6$), in which the glass-forming metalloid is replaced by a nontransition metal has been reported.[7] Bulk magnetization measurements show that substitution of Be for B causes an initial increase in saturation magnetization at 4.2 K, followed by a decrease for alloys with more than 4 at.% Be. The concentration dependence of the Curie temperature (T_c) indicates that T_c decreases progressively with the Be content. The results of annealing experiments indicate there are two crystallization stages for every alloy except $Fe_{82}B_{18}$. In the present work amorphous $Fe_{82}B_{18-x}Be_x$ ($0 \leq x \leq 6$) is studied by ^{57}Fe Mössbauer spectroscopy. The distribution function of the effective magnetic hyperfine field, $P(H)$, and its characteristic parameters are determined for each composition x. The crystalline phases which precipitate out from the annealed samples are identified. The results and their implications are discussed qualitatively.

II. EXPERIMENTAL

Amorphous ribbons were prepared by quenching the melt onto a rotating copper wheel.[7] The glassy, as-quenched ribbons 2 mm wide, 15 mm long, and approximately 0.02 mm thick, were placed parallel to each other and attached to a plastic substrate by vacuum grease and used as absorbers. In the annealing experiments ribbons were sealed into a quartz tube and after evacuating down to 2×10^{-7} Torr were placed in a preheated furnace for 2–3 h. For low-temperature measurements the ribbons were held in place on a beryllium disk by vacuum grease and clamped onto a copper rod which was connected to the liquid-nitrogen reservoir in a stainless-steel cryostat with a beryllium window.

The Mössbauer spectra were obtained with a Ranger Electronics spectrometer coupled with a TMC 1024-channel analyzer operated in both constant acceleration and region of interest (ROI) modes. An Armco iron foil was used in velocity calibration. A typical iron spectrum has an inner linewidth of 0.25 mm/sec and an isomer shift of −0.214 mm/sec relative to the source at room temperature. The source is 11.5 mCi ^{57}Co in copper matrix with a linewidth of 0.107 mm/sec. All the spectra taken throughout the experiments contained approximately (150–450) $\times 10^3$ counts per channel in each 1024-channel spectrum.

III. RESULTS AND DISCUSSION

A. Hyperfine-field distribution and isomer shift

Typical Mössbauer spectra of metallic glasses $Fe_{82}B_{18-x}Be_x$ taken at room temperature and liquid-nitrogen temperatures are shown in Fig. 1. All the spectra exhibit linewidths which are much wider than those of crystalline solids. The usual fit of six Lorentzian lines yields typical linewidths of the outer lines of 1.46 and 1.25 mm/sec and typical linewidths of the inner lines of 0.56 and 0.37 mm/sec for spectra taken at liquid-nitrogen and room temperatures, respectively. However, the linewidths of the middle lines remain around 0.85 mm/sec at both temperatures. The strong line broadening results from the distribution of hyperfine fields, isomer shifts, and quadrupole splittings and reflects the strong variations in the strength of the hyperfine interactions due to different Fe atom environments in the amorphous state. Since the fit to six Lorentzian lines can only give the average effective magnetic hyperfine field, $\bar{H}_{\text{eff}}$, and the average isomer shift, $\bar{\delta}$, the data were analyzed by means of a procedure developed by Window.[8] In this method, the Mössbauer spectra were unfolded to yield the distribution function of the effective magnetic field $P(H)$ by Fourier expansion.

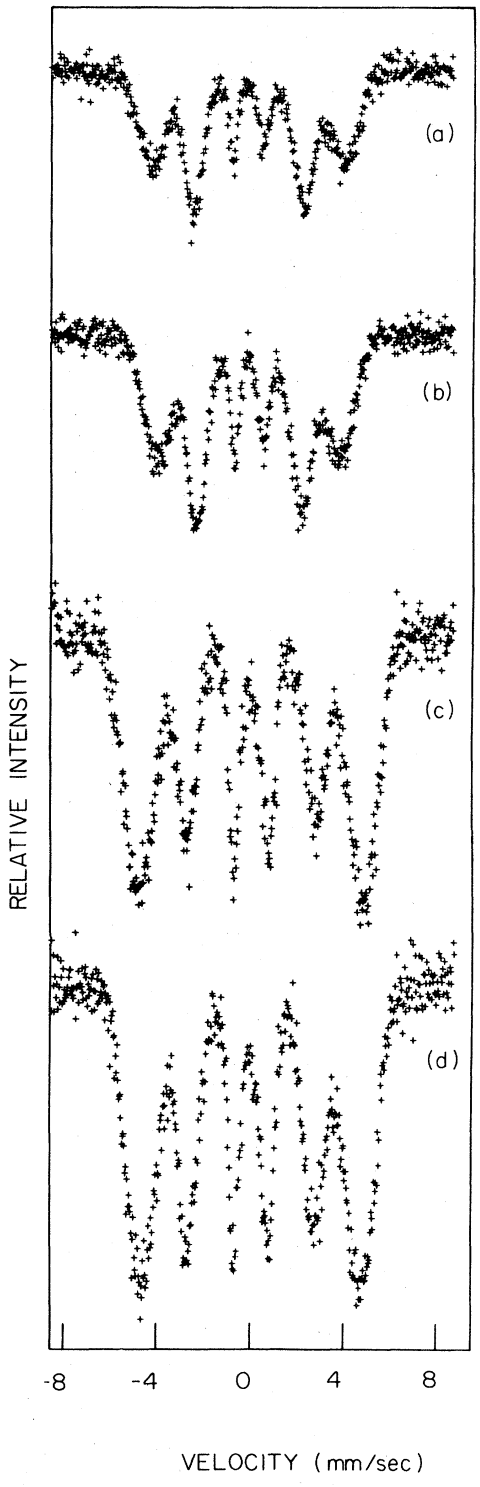

FIG. 1. ^{57}Fe Mössbauer spectra of amorphous (a) $Fe_{82}B_{14}Be_4$, (b) $Fe_{82}B_{13}Be_5$ at room temperature; (c) $Fe_{82}B_{14}Be_4$, (d) $Fe_{82}B_{13}Be_5$ at liquid-nitrogen temperature.

This method requires that quadrupole interactions are negligible and isomer shift effects small. It is understood that in the magnetically ordered state of an amorphous magnetic solid there is almost no apparent quadrupole interaction.[3] Also, the experimental results on intermetallic compounds of transition metals with metalloids show only minor changes in the isomer shift.[9] As a first approximation, the severe line broadening present in the spectra will mask any measurable effects due to isomer shifts. Therefore, Window's method of analysis should provide a relatively good description of the experimental Mössbauer spectra of metallic glasses.

Spectra of amorphous $Fe_{82}B_{18-x}Be_x$ $(0 \leq x \leq 6)$ at liquid-nitrogen temperature were analyzed using Window's method. The resultant $P(H)$ vs H curves for different Be contents are shown in Fig. 2. The oscillatory features of the $P(H)$ in the high- and low-field regions are the result of truncated Fourier analysis and should not be considered as physically meaningful. In this analysis we use $N=15$ and $H_{max}=525$ kOe which should provide good description of the experimental data,[3] where N is the number of terms in the truncated Fourier analysis and H_{max} is a chosen value at which $P(H_{max})=0$. The observed $P(H)$ at liquid-nitrogen temperature are characterized by well-defined, symmetric and single-maximum functions of H. The shapes of $P(H)$ are similar and not very sensitive to the Be content, but the most probable value of the effective magnetic hyperfine field, H_1, shifts to larger values of H initially and subsequently begins to decrease as the Be content increases above 4 at.%. The $P(H)$ curves at room temperature for different Be concentrations are shown in Fig. 3 for comparison. Note that the shape of $P(H)$ shows very little change as temperature increases from liquid-nitrogen to room temperature. The width of $P(H)$, ΔH, remains essentially constant at a value of 80 kOe. However, H_1 shifts to the lower value considerably. The differences in effective magnetic hyperfine field between liquid-nitrogen and room temperature are very large compared to those of crystalline ferromagnetic materials. For example, $H_1=300$ and 260 kOe for the metallic glass $Fe_{82}B_{14}Be_4$ at liquid-nitrogen temperature and room temperature, respectively. On the other hand, there is a change of only 7 kOe in the effective magnetic hyperfine field in iron metal under similar temperature variation. This results from the fact that more spin waves of long wavelengths are excited in amorphous ferromagnets than in crystalline ferromagnets.[3]

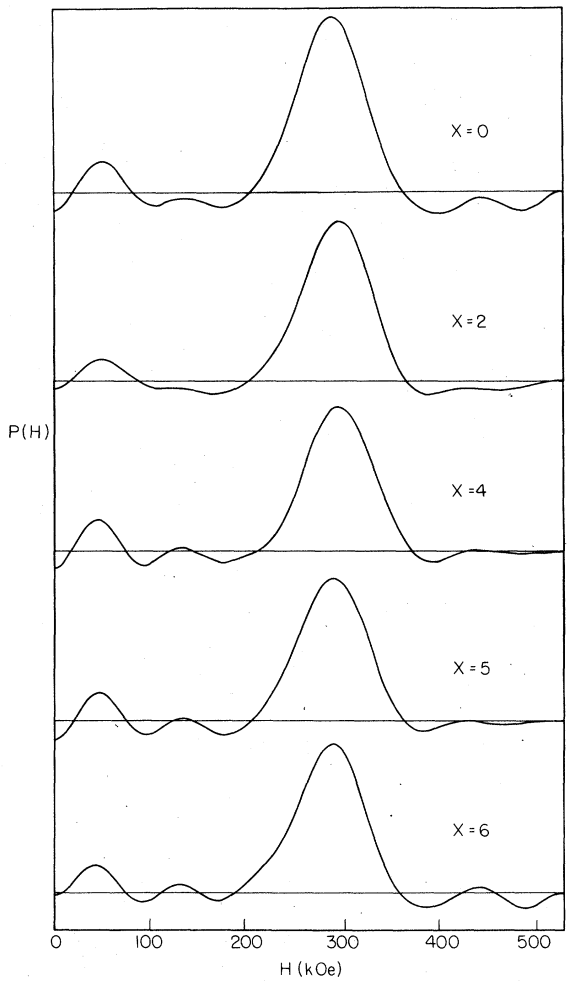

FIG. 2. ^{57}Fe hyperfine field distributions of amorphous $Fe_{82}B_{18-x}Be_x$ $(0 \leq x \leq 6)$ at liquid-nitrogen temperature.

The $P(H)$ can be characterized by the parameters H_1 and ΔH. The concentration dependence of these parameters is given in Fig. 4. Also shown in this figure are H_m and H_M, the effective magnetic hyperfine fields at which the value of $P(H)$ approaches zero on the low-field and high-field side of the distribution function, respectively. For comparison, the effective magnetic hyperfine field, $\bar{H}_{eff}$, obtained by using six Lorentzian lines is also included in the figure. The $\bar{H}_{eff}$ is always several kOe smaller than H_1 due to the different methods of data analysis. One can observe from this plot that all parameters except ΔH, which remains constant, follow a similar trend as the Be content x changes. It is quite interesting that H_M has a value considerably larger than 340 kOe, the saturation value of the effective magnetic hyperfine field of iron metal, for all samples we investigated.

The average magnetic moment per Fe atom, $\bar{\mu}_{Fe}$, in metallic glasses $Fe_{82}B_{18-x}Be_x$ at 4.2 K has been measured[7] previously. The substitution of Be for B in the amorphous binary $Fe_{82}B_{18}$ caused an initial increase in $\bar{\mu}_{Fe}$ to a maximum of $2.21\mu_B$ followed by a decrease for alloys with more than 4 at.% Be. This behavior is quite similar to the $P(H)$ curve we ob-

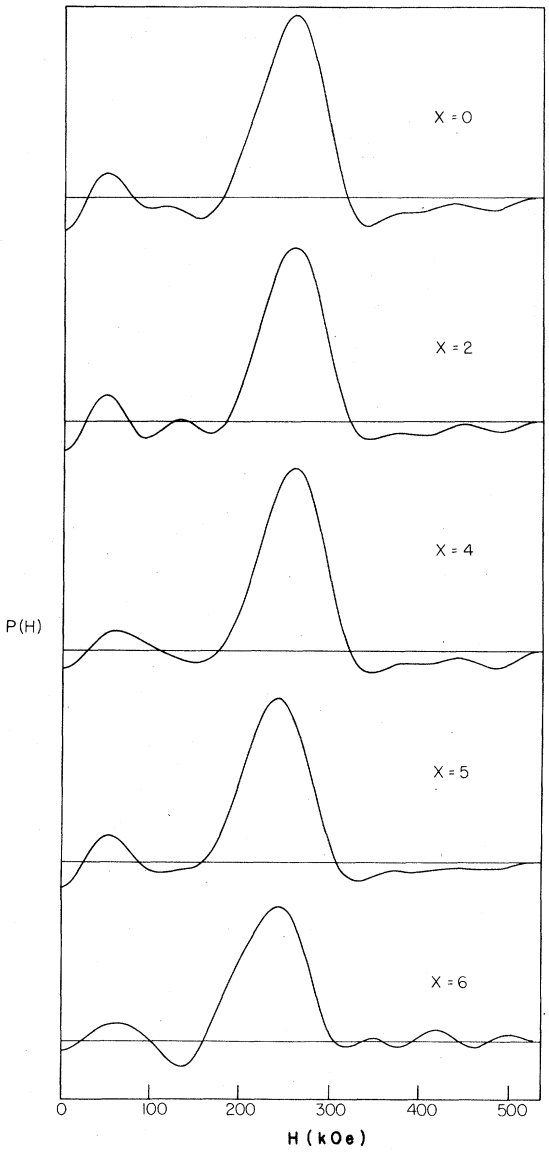

FIG. 3. ^{57}Fe hyperfine field distributions of amorphous $Fe_{82}B_{18-x}Be_x$ ($0 \leq x \leq 6$) at room temperature.

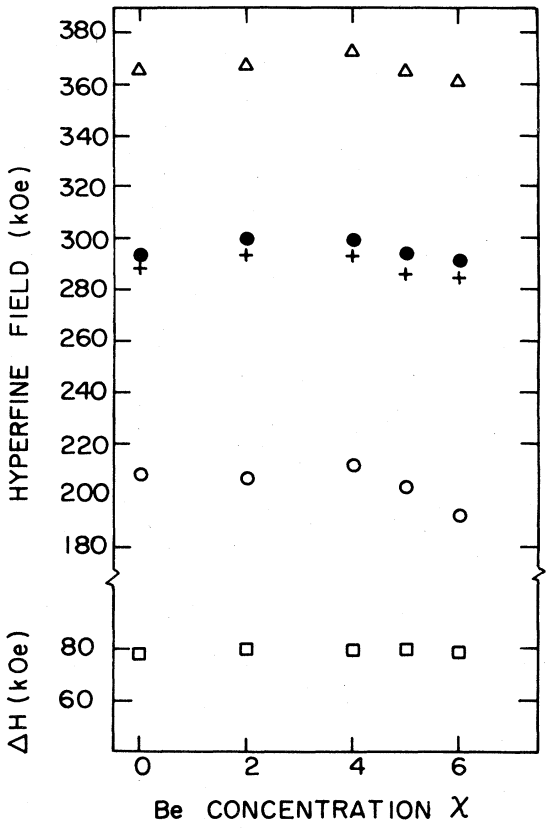

FIG. 4. Concentration dependence of the various parameters of the ^{57}Fe hyperfine field distribution function $P(H)$ in amorphous $Fe_{82}B_{18-x}Be_x$ ($0 \leq x \leq 6$) at liquid-nitrogen temperature: Δ, H_M; $\bullet, H_1$; $+, \bar{H}_{\text{eff}}$; $\circ, H_m$; $\square, \Delta H$.

served in this Mössbauer study. For example, the H_1 values increase from 293 kOe for the $Fe_{82}B_{18}$ alloy to 300 kOe for the $Fe_{82}B_{14}Be_4$ alloy and then drop down to 291 kOe for the $Fe_{82}B_{12}Be_6$ alloy. The nearly proportional behavior of $\bar{\mu}_{\text{Fe}}$ and $\bar{H}_{\text{eff}}$ has also been found in other Fe-based metallic glasses[5,10] and other crystalline Fe-metalloid compounds.[11] This is considered to be a result of the small polarization of 4s-like conduction electrons in these alloys. For Fe and its alloys in which the orbital angular momentums of the 3d electrons are quenched[12,13] the dominant Fermi-contact interaction involving core electrons contributes negatively to $\bar{H}_{\text{eff}}$, whereas the polarization of 4s electrons contributes positively. As a result of the negligible contribution from 4s-like conduction-electron polarization, it is reasonable that some Fe sites in the $Fe_{82}B_{18-x}Be_x$ metallic glasses have $\bar{H}_{\text{eff}}$ greater than the saturation value of the effective magnetic hyperfine field of Fe.

Structural analyses by x-ray diffraction of many metallic glasses have indicated that the atomic distribution can be modeled[1,14] as a dense random packing of spheres (DRPS). In the Fe_xB_{100-x} binary metallic glasses the results[14] of computationally simulated DRPS model indicated that on the average nearest-neighbor coordination number of B atoms around an Fe site decreases as the B concentration x decreases, but those of Fe atoms remain nearly constant. Experimentally determined $\bar{H}_{\text{eff}}$ (Ref. 10) and $\bar{\mu}_{\text{Fe}}$ (Refs. 15 and 16) all showed that these physical quantities decrease monotonically as the B content increases in metallic glasses of the Fe_xB_{100-x} ($72 \leq x \leq 86$) system. It has been empirically established that in the ferromagnetic Fe-metalloid alloys,

both the $\bar{H}_{\text{eff}}$ at Fe sites and the magnetic moments are mainly determined by the number of nearest metalloid neighbors, irrespective of the state of crystallinity.[17,18] Qualitatively speaking, the more metalloid atoms exist in the nearest neighbors of Fe sites the smaller $\bar{H}_{\text{eff}}$ and $\bar{\mu}_{\text{Fe}}$ are. Haydock and You[19] used the local environment approach[20] to calculate local densities of states (LDOS) of different Fe sites in ordered Fe_3Al and then used these LDOS within the context of the Stoner theory to calculate the moment at individual Fe sites. The results are in good agreement with experiments. Qualitatively, the longer the states near the Fermi surface are atomiclike the larger the exchange energy relative to the kinetic energy and hence the larger the moment that will occur. The lifetime of an electron in an atomiclike state depends on how strongly this state is coupled to the states on neighboring atoms. The degree of coupling will depend on the nature and number of neighboring atoms. In Fe-metalloid alloys the metalloid elements are precisely those with strongly interactive *sp* electrons. These elements usually form delocalized *sp* valence bands in the solid form. The decrease of $\bar{\mu}_{\text{Fe}}$ as well as of $\bar{H}_{\text{eff}}$ in Fe_xB_{100-x} ($72 \leq x \leq 86$) metallic glasses with increasing x can be explained qualitatively by this local environment approach. Since the Be atom has one *sp* electron less than the B atom, as the Be content increases in $Fe_{82}B_{18-x}Be_x$ metallic glasses, the Fe atoms occur in relatively more isolated environments. The consequences are that the states near the Fermi level will be relatively more localized and hence will have relatively larger exchange splitting and a higher value of $\bar{H}_{\text{eff}}$. However, for samples with $x > 4$, $\bar{H}_{\text{eff}}$ decreases instead of increasing as expected because of fewer electrons in the surrounding Fe sites with which to intereact.

The isomer shift shown in Fig. 5 has a value of -0.032 mm/sec for samples with $x \leq 4$ but changes to -0.050 mm/sec for samples with $x > 4$. This indicates that the *s*-electron density at the ^{57}Fe nucleus is higher for $x > 4$ samples than at those of $x \leq 4$ samples and, in turn, suggests that local environments around the Fe atoms undergo significant changes as x is increased from 4 to 5. This correlates very well with results of Be Auger analysis that the Be Auger *KVV* transition occurs at 92.3 eV for $x \leq 4$ samples and at an energy of 106.2 eV for $x > 4$.[21] In addition, data of mass density, magnetostriction, and saturation magnetization on fully noncrystalline $Fe_{80}B_{20-x}Be_x$ ($0 \leq x \leq 12$) measured by Hasegawa[22] also have similarly different behaviors for $x > 4$ and ≤ 4. Hasegawa attributes these effects to different site occupancies of Be atoms in the alloys, namely, below 4 at.% the Be atoms occupy sites similar to those of Fe atoms but above 4 at.% occupy sites similar to those of B atoms. Unfortunately, direct investigation of local coordination numbers on B and Be are very difficult due to the small x-ray scattering cross sections and relatively small amounts of B and Be atoms compared to Fe in the alloys.

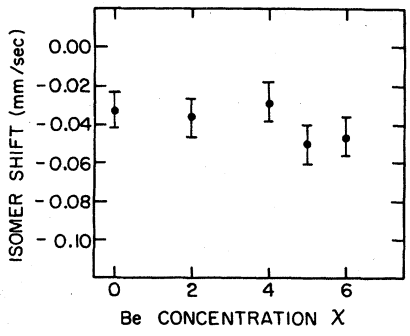

FIG. 5. Concentration dependence of the ^{57}Fe isomer shift in $Fe_{82}B_{18-x}Be_x$ ($0 \leq x \leq 6$) at liquid-nitrogen temperature.

B. Analysis of crystallization products

It was found[7] that the effect on crystallization behavior on substitution of Be for B in $Fe_{82}B_{18}$ metallic glasses is to change from a single crystallization stage to 2. Figure 6(a) shows the room-temperature Mössbauer spectrum of $Fe_{82}B_{18}$ sample annealed for 3 h at $T_a = 420\,^{\circ}\text{C}$, which is about 20 °C higher than the crystallization temperature. The spectrum clearly indicates that besides the well-known six-line pattern of α-Fe, there is a second phase with a somewhat more complicated spectrum. By subtracting the six α-Fe lines the spectrum of the second phase is obtained and is shown in Fig. 6(b). This spectrum is identical to the published spectrum of the tetragonal Fe_3B phase.[10] It has been shown[10] that at a high heating rate as has been used in the present experiment, the main crystalline phase of amorphous Fe_xB_{100-x} is the tetragonal Fe_3B.

Shown in Fig. 7 are typical spectra of annealed samples of Be-substituted $Fe_{82}B_{18}$. The annealing temperature is 420 °C which is above the first crystallization temperature, T_{x1}, but lower than the second crystallization temperature, T_{x2}. All of the spectra consist of six sharp α-Fe lines plus six more well-defined but broadened lines. However, at the region near the inner side of the α-Fe outer lines there appear extra lines with relatively low intensity. Similar spectra were obtained after annealing the $x = 6$ sample for 12 h at 420 °C and the $x = 2$ sample for 2 h at 485 °C which is near T_{x2}. These satellite lines are the characteristic features of solute atoms located in substitutional sites of dilute iron-based alloys.[23–25] Since the solubility of B in α-Fe is very low,[26] and no similar satellite lines were found in the crystallization study of Fe_xB_{100-x} metallic glasses,[5] it

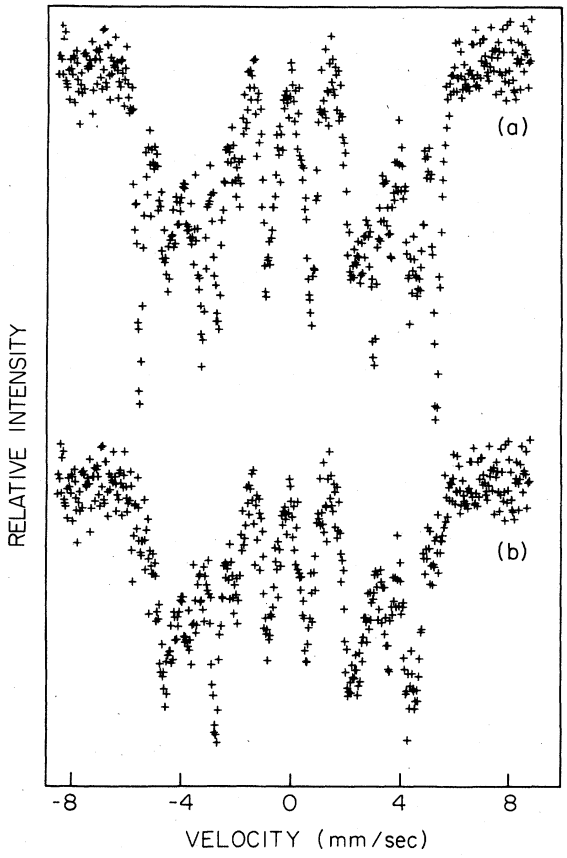

FIG. 6. (a) ^{57}Fe Mössbauer spectrum of amorphous $Fe_{82}B_{18}$ at room temperature after annealing at $T_a = 420\,^{\circ}C$ for 3 h. (b) The spectrum of the remaining phase after subtracting the α-Fe contribution.

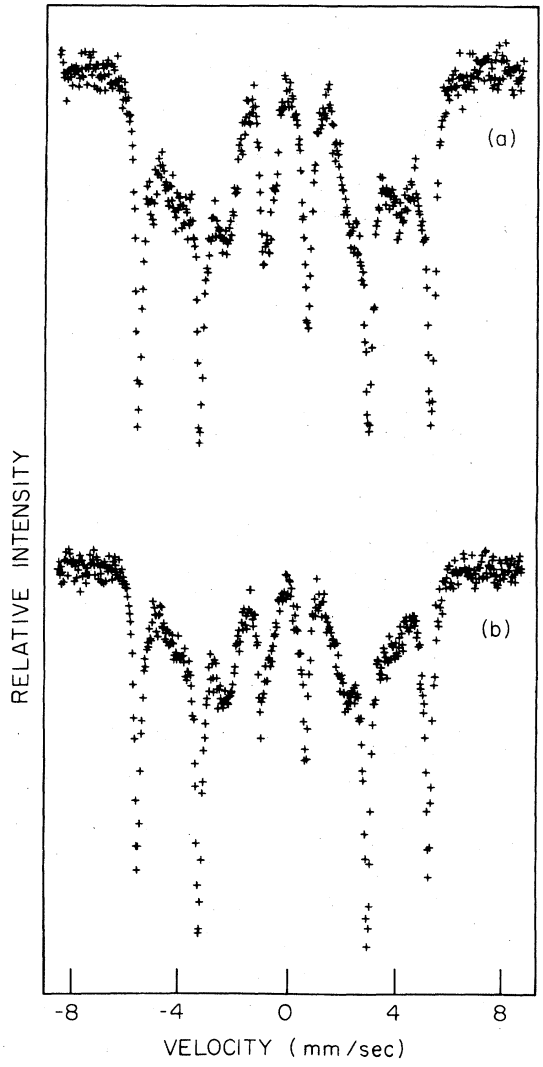

FIG. 7. ^{57}Fe Mössbauer spectra of amorphous (a) $Fe_{82}B_{14}Be_4$, (b) $Fe_{82}B_{13}Be_5$, at room temperature after annealing at $T_a = 420\,^{\circ}C$ for 3 h.

is reasonable to attribute these satellite lines to the effect of Be atoms replacing Fe atoms in the α-Fe phase formed upon annealing above T_{x1}. In order to obtain better resolution, room-temperature Mössbauer spectra of annealed samples were obtained using the region of interest mode (ROI). In the ROI mode of operation, velocity was scanned effectively only through the ranges which contain the outer four lines of the iron spectrum. Typical spectra are shown in Fig. 8. The velocity is approximately 0.0088 mm/sec channel. These ROI spectra show that the satellite lines have different intensities for different samples. Also shown in Fig. 8 are the spectra of crystalline α-Fe solid solutions with 3 and 7 at.% Be prepared for comparison. Because only the effects of first-nearest neighbor substitutions can be reliably determined,[24,25] only one satellite line is assumed near each of the Fe outer lines. By measuring the distances between the outer Fe lines and the satellite lines the change of $\bar{H}_{\rm eff}$ due to Be substitution was determined to be -18 ± 3 kOe which is close to the published value.[24] Therefore, upon annealing samples between T_{x1} and T_{x2} the first crystalline phase that can be identified by Mössbauer spectroscopy is the Fe-Be solid solution.

To determine quantitatively the compositions of these Fe-Be solid solutions, it is assumed that Be atoms distribute randomly in the bcc α-Fe lattice. The intensity ratio of the satellite line and the corresponding outer Fe line depends on the composition of the solid solution. The probability that an iron atom has n Fe nearest neighbors for a given concentration c of Be randomly distributed in the bcc Fe lattice is given by

$$P(c,n) = \binom{8}{n}(1-c)^n c^{8-n} \quad . \tag{1}$$

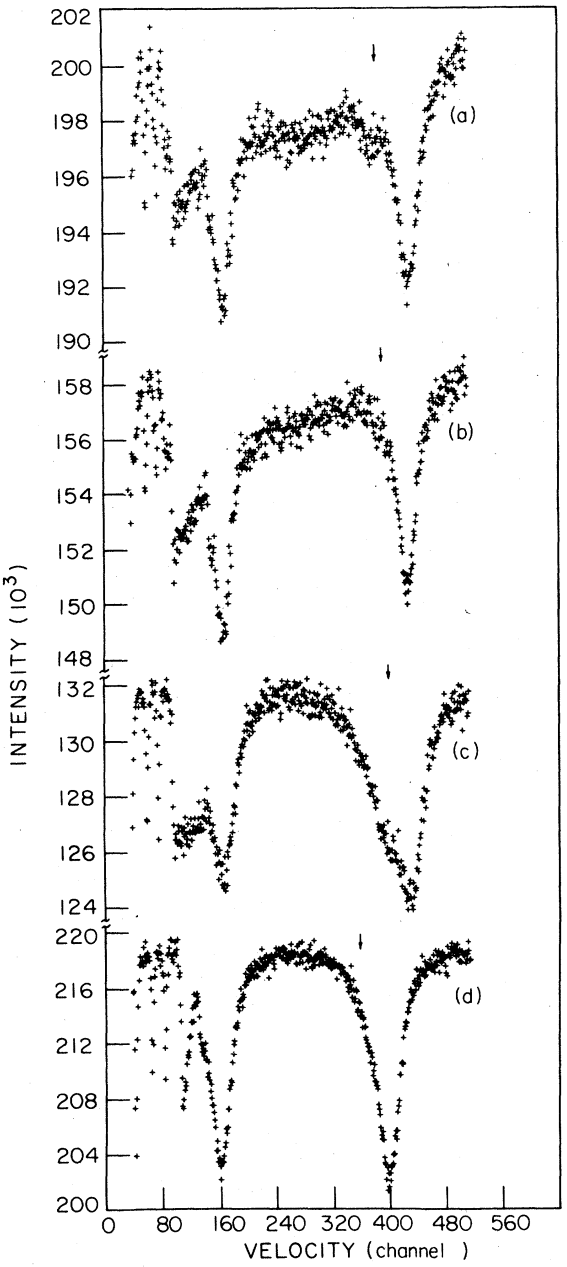

FIG. 8. ROI ^{57}Fe Mössbauer spectra of amorphous (a) $Fe_{82}B_{14}Be_4$, (b) $Fe_{82}B_{13}Be_5$, at room temperature after annealing at $T_a = 420\,^{\circ}C$ for 3 h and of (c) $Fe_{93}Be_7$, (d) $Fe_{97}Be_3$. The spectra shown are the portions between the iron metal outer and middle lines in the negative velocity region. The extra peak indicated by the arrow near the outer line is the satellite line.

The experimentally determined and calculated intensity ratios are tabulated in Table I. By comparing these ratios the composition c is determined for each annealed sample and is also shown in the table. For simplicity, only the effects of nearest neighbors are taken into account and it is assumed that only one satellite line occurs near the outer Fe line. This method of analysis gives good agreement between calculated and experimentally determined ratios for the samples $Fe_{93}Be_7$ and $Fe_{97}Be_3$ which were prepared for comparison. It is quite interesting that the thus-obtained c values for the $x = 2, 4$ samples are greater than the x values but for the $x = 5, 6$ samples they are smaller. According to the reaction scheme, for example

$$Fe_{82}B_{13}Be_5 \rightarrow y\,Fe_{96.5}Be_{3.5} + Fe_{82-96.5y}B_{13}Be_{5-3.5y} \ , \quad (2)$$

it is impossible to obtain a physically meaningful value of y for the $x = 4, 5, 6$ samples if no Be is in the remaining phase unless there are additional phases X present which are not detected by ^{57}Fe Mössbauer spectroscopy. However, x-ray diffraction was not able to provide any evidence for the X phase or phases. Therefore, the remaining phase characterized by the six broadened lines in the obtained Mössbauer spectra is a metastable amorphous phase of Fe-B-Be.

For the metastable amorphous state formed upon annealing between T_{x1} and T_{x2} the $\bar{H}_{\rm eff}$ and isomer shift are plotted in Fig. 9 for both room temperature and liquid-nitrogen temperature. These results were obtained by fitting the Mössbauer spectra with two sets of six Lorentzian lines and ignoring the contributions of the satellite lines. Any attempt to fit the data with more than two sets of six Lorentzian lines only introduces too many parameters and yields physically unreasonable results. Using three sets of six Lorentzian lines with additional constraints give no better fit than that of two sets of six Lorentzian lines. From Figs. 5 and 9 one can see that the isomer shifts increase positively relative to those for the as-quenched samples. This is due to an increase of the B concentration in the remaining metastable amorphous phase as Fe and Be precipitate out upon annealing. It is consistent with the experimental data[10] that in Fe-B binary metallic glasses the isomer shift increases positively as the B concentration increases. The $\bar{H}_{\rm eff}$ decreases relative to the values of as-quenched samples for the same reason that more B atoms are nearest neighbors of Fe in the metastable amorphous phase. Attempts to determine the exact compositions of these metastable states by means of the Mössbauer effect were hampered by the very different Mössbauer fractions of the crystalline and amorphous phases.

Figure 10 shows some Mössbauer spectra for samples annealed for 2 h at 485 °C which is about 15 to 20 °C above T_{x2}. All these spectra show sharply defined lines. The wider six-line pattern with satellite lines is the Fe-Be solid solution. The six-line pattern with smaller splitting is due to Fe_2B and has an $\bar{H}_{\rm eff}$ of 236 kOe and an isomer shift of −0.10 mm/sec. The ROI spectra of these are shown in Fig. 11. These spectra resemble those shown in Fig. 8, the only difference being the slightly smaller intensity ra-

TABLE I. (a) Calculated occupation probability ratios of with and without Be located in nearest-neighbor substitutional sites of an iron atom. Here, c denotes the concentration of Be in Fe-Be solid solution phase. (b) Experimentally determined intensity ratios of the satellite lines and corresponding outer Fe line and the estimated concentration of Be in the Fe-Be solid solution which has precipitated out after annealing the as-quenched ribbons between T_{x1} and T_{x2}.

c(%)	2	3	3.5	4	4.5	5	6	7
$\frac{P(c,7)+P(c,6)}{P(c,8)}$	0.176	0.276	0.327	0.400	0.439	0.501	0.625	0.754

(a)

Alloy	$x=2$	$x=4$	$x=5$	$x=6$	$Fe_{97}Be_3$	$Fe_{93}Be_7$
$\frac{I_S}{I_{Fe}}$	0.510	0.429	0.325	0.504	0.280	0.749
Estimated c(at.%)	5	4.5	3.5	5	3	7

(b)

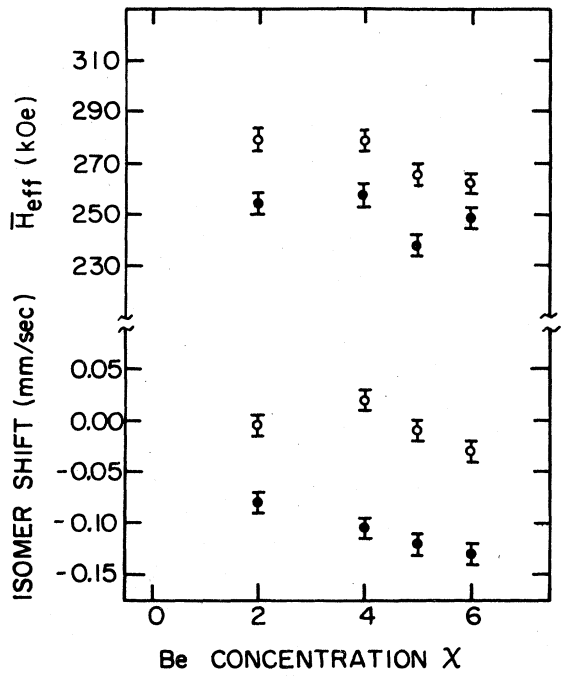

FIG. 9. Concentration dependence of ^{57}Fe $\bar{H}_{eff}$ and isomer shift in the remaining metastable phase after annealing the as-quenched ribbons of amorphous $Fe_{82}B_{18-x}Be_x$ ($2 \leq x \leq 6$) between T_{x1} and T_{x2}: ○ liquid-nitrogen temperature, ● room temperature.

tio between the satellite line and the outer Fe line due to more Fe precipitating out from the metastable amorphous phase.

For the 14.4-keV state of ^{57}Fe the relative intensities of Mössbauer lines have ratios of $3:4\sin^2\theta/(1+\cos^2\theta):1$ where θ is the angle between the direction of $\bar{H}_{eff}$ and the incoming γ ray. Therefore, by comparison of the relative intensities of the outer and middle lines of spectra the direction of $\bar{H}_{eff}$ can be determined. The spectra shown in Figs. 7 and 10 indicate that samples annealed above T_{x2} have stronger intensities in the middle lines instead of in the outer lines of the α-Fe six-line patterns. On the other hand the opposite is true for samples annealed between T_{x1} and T_{x2}. The area ratios of the three pairs of lines in the α-Fe Mössbauer spectra are close to 3:2:1 for samples annealed above T_{x2} but close to 3:3.1:1 for samples annealed between T_{x1} and T_{x2}. These correspond to a completely random orientation of $\bar{H}_{eff}$ in the former case but nearly perpendicular to the γ-ray direction for the latter. These changes of orientation of $\bar{H}_{eff}$ are not difficult to understand. Since the samples annealed above T_{x2} are completely random microcrystallites of α-Fe and Fe_2B and since the strains frozen in the samples during the rapid quenching process were fully released, the magnetization direction will be randomly oriented. However, samples annealed between T_{x1} and T_{x2} still have the metastable amorphous phase dispersed in the samples

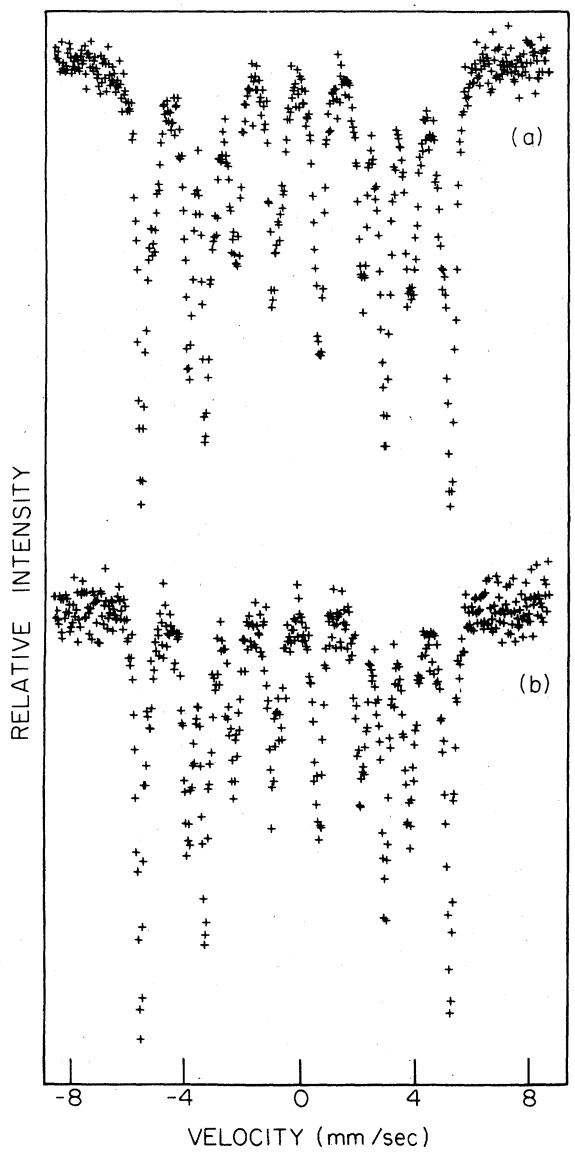

FIG. 10. ^{57}Fe Mössbauer spectra of amorphous (a) $Fe_{82}B_{14}Be_4$, (b) $Fe_{82}B_{13}Be_5$ at room temperature after annealing at $T_a = 485\,^{\circ}C$ for 2 h.

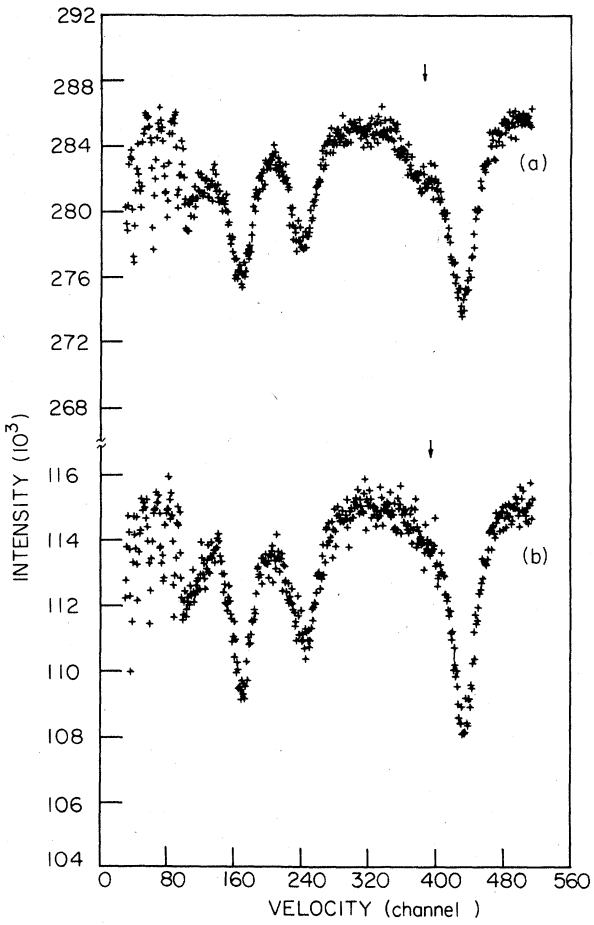

FIG. 11. ROI ^{57}Fe Mössbauer spectra of amorphous (a) $Fe_{82}B_{14}Be_4$ and (b) $Fe_{82}B_{13}Be_5$ at room temperature after annealing at $T_a = 485\,^{\circ}C$ for 2 h. The spectra shown are the portions between the iron metal outer and middle lines in the negative velocity region. The extra peak indicated by the arrow near the outer line is the satellite line.

and, consequently, the magnetization direction remains close to the ribbon plane.

IV. SUMMARY AND CONCLUSION

^{57}Fe Mössbauer spectra have been obtained at liquid-nitrogen temperature for a series of metallic glasses $Fe_{82}B_{18-x}Be_x$ ($0 \leq x \leq 6$). The distribution functions of the effective magnetic hyperfine field $P(H)$ for these metallic glasses show a well-defined and symmetric shape. The width of $P(H)$, ΔH, remains approximately constant at a value of 80 kOe for all samples. However, the most probable value of the effective magnetic hyperfine field, H_1, initially increases with x, but starts decreasing as x becomes greater than 4. The isomer shift has a value of -0.032 mm/sec for samples with $x \leq 4$ but changes to -0.050 mm/sec for samples with $x > 4$.

The crystallization product obtained upon annealing the $Fe_{82}B_{18}$ metallic glass at $T_a = 420\,^{\circ}C$ was identified as tetragonal Fe_3B and α-Fe. However, annealing the samples with $x > 0$ between T_{x1} and T_{x2} yields crystallized solid solutions of an Fe-Be phase and a metastable amorphous phase. The compositions of these Fe-Be solid solutions were determined from the intensity ratio of the satellite lines and outer α-Fe lines

of Mössbauer spectra obtained by using the spectrometer in the ROI mode. The metastable phase has a more negative isomer shift and a smaller $\overline{H}_{\text{eff}}$ than those for the as-quenched ribbons due to the increased B concentration. The direction of $\overline{H}_{\text{eff}}$ in these samples was determined to be close to the ribbon plane due to the remaining frozen strain in the metastable phase.

Annealing the $x > 0$ samples at temperatures higher than T_{x2} produced only crystallized phases. Mössbauer spectra indicate that one phase is the Fe-Be solid solution and the other is Fe_2B. The direction of $\overline{H}_{\text{eff}}$ was determined to be randomly oriented due to the complete release of frozen strain.

ACKNOWLEDGMENTS

Ames Laboratory is operated for the U.S. Department of Energy by Iowa State University under Contract No. W-7405-Eng-82. This research was supported by the Director for Energy Research, Office of Basic Energy Sciences, WPAS-KC-02-02-02.

[1]Y. Weseda, H. Okazaki, and T. Masumoto, J. Mater. Sci. 12, 1927 (1977).
[2]P. H. Gaskell, J. Noncryst. Solids 32, 207 (1979).
[3]C. L. Chien, Phys. Rev. 18, 1003 (1978).
[4]A. Amamou, Phys. Status Solidi (a) 54, 565 (1979).
[5]C. L. Chien, D. Musser, F. E. Luborsky, and J. L. Walter, J. Phys. F 8, 2407 (1978).
[6]T. Kemény, I. Vincze, B. Fogarassy, and Sigurds Arajs, Phys. Rev. B 20, 476 (1979).
[7]C. S. Severin, C. W. Chen, A. J. Bevolo, and M. C. Lin, J. Appl. Phys. 52, 1850 (1981).
[8]B. Window, J. Phys. E 4, 401 (1971).
[9]I. Vincze, M. C. Cadeville, R. Jesser, and J. Takács, J. Phys. (Paris) 35, C6-533 (1974).
[10]C. L. Chien, D. Musser, E. M. Gyorgy, R. C. Sherwood, H. S. Chen, F. E. Luborsky, and J. L. Walter, Phys. Rev. B 20, 283 (1979).
[11]H. Bernas, I. A. Campbell, and R. Fruchart, J. Phys. Chem. Solids 28, 17 (1967).
[12]K. J. Duff and T. P. Das, Phys. Rev. B 3, 192 (1971).
[13]R. E. Watson and A. J. Freeman, Phys. Rev. 123, 2027 (1961).
[14]D. S. Boudreaux, Phys. Rev. B 18, 4039 (1978).
[15]R. Hasegawa and R. Ray, J. Appl. Phys. 49, 4174 (1978).
[16]F. E. Luborsky, H. H. Liebermann, J. J. Becker, and J. L. Walter, in *Rapidly Quenched Metals III*, edited by B. Cantor (The Metals Society, London, 1978), pp. 188–197.
[17]I. Vincze, D. S. Boudreaux, and M. Tegze, Phys. Rev. B 19, 4896 (1979).
[18]M. E. Lines, Solid State Commun. 36, 457 (1980).
[19]R. Haydock and M. V. You, Solid State Commun. 33, 299 (1980).
[20]V. Heine, *Solid State Physics* (Academic, New York, 1980), Vol. 35.
[21]A. J. Bevolo, C. S. Severin, and C. W. Chen (unpublished).
[22]R. Hasegawa, J. Appl. Phys. 52, 1847 (1981).
[23]G. K. Wertheim, V. Jaccarino, J. H. Wernick, and D. N. E. Buchanan, Phys. Rev. Lett. 12, 24 (1964).
[24]I. Vincze and A. T. Aldred, Solid State Commun. 17, 639 (1975).
[25]I. Vincze and A. T. Aldred, Phys. Rev. B 9, 3845 (1974).
[26]Hansen, *Constitution of Binary Alloys*, 2nd ed. (McGraw-Hill, New York, 1958).